

Spectroscopy of Francium Isotopes

J. S. Grossman, L. A. Orozco, M. R. Pearson and G. D. Sprouse

Department of Physics and Astronomy, State University of New York, Stony Brook, NY 11794-3800, U.S.A.

Received September 2, 1999; accepted December 2, 1999

PACS Ref: 32.30.-r, 32.70.Cs, 32.10.Fn, 31.30.Gs

Abstract

We have performed precision spectroscopy on cold francium atoms in a magneto optical trap. Our measurements test the present *ab initio* calculations for the understanding of the electronic structure of the atom. We probe the distribution of the nuclear magnetization through measurements of the $7P_{1/2}$ hyperfine splitting in a chain of neutron deficient francium isotopes.

1. Introduction

Francium is the heaviest of the alkali elements and has no stable isotopes. As such it is the simplest-heavy atom to study spectroscopically. It occurs naturally from the α decay of actinium or artificially from fusion or spallation nuclear reactions. Its longest lived isotope, ^{223}Fr , has a half-life of 22 minutes. Previously, experiments to study the atomic structure of francium were possible only with the very high fluxes available at a few facilities in the world such as ISOLDE at CERN, or by use of natural sources. Nowadays it is possible to capture francium atoms in a magneto-optical trap and study their spectroscopy. Francium is now the grounding test of many-body perturbation theory (MBPT), and we hope to use it to study parity non-conservation in atoms.

1.1 History

Marguerite Perey [1], of the Curie Institute in Paris, reported in 1939 the discovery of a new radioactive element. While doing chemical analysis of the decay products of actinium, she found an element that behaved as an alkali. She named the new element francium after her country.

The study of its atomic spectroscopy has been limited by the availability of francium. During the 1970s and 1980s a team led by the late Sylvain Liberman [2] found the D_2 line of Fr and then proceeded to study further its atomic structure. They produced francium at CERN using the isotope separator ISOLDE. The result after some ten years of experiments was a map of the energy levels and the hyperfine structure of the different isotopes [3]. The group of Letokhov from Moscow University [4] used a radioactive source to study some more the properties of highly excited states of francium.

Since 1995 we have captured francium in a magneto optical trap (MOT) [5] at Stony Brook. We can produce and trap five of the neutron deficient isotopes. More recently, the collaboration between the groups of Wieman from the University of Colorado and Gould from the Lawrence Berkeley Laboratory trapped ^{221}Fr [6] from a radioactive source in a MOT.

1.2 Motivation

The large number of constituent particles in the francium atom makes electron correlations and relativistic effects important.

However, its structure is calculable with many-body perturbation theory (MBPT). The more than two hundred nucleons make it an attractive candidate for a future atomic parity non-conservation (PNC) experiment. The PNC effect is predicted to be 18 times larger in Fr than in Cs [7].

Francium is an excellent element for understanding the atom-nucleus hyperfine interactions, and eventually weak interactions. First, because of the large Z , hyperfine effects proportional to Z^3 are larger than in lighter atoms. Second, the simple atomic structure allows *ab initio* calculations of its properties [7, 8, 9], as well as other model calculations [10, 11], that have been experimentally tested [13]. Third, Fr has a large number of isotopes spanning almost 30 neutrons with lifetimes greater than 1 second that cover a wide range of nuclear structure.

2. Production and Capture

In this section we review some of the requirements for trapping radioactive Fr. The interested reader should look at Ref. [14], a review article that has a section on this subject. We begin with a discussion of the target. Gold is ideal for francium production because it is chemically inert, has clean surfaces, and a low vapor pressure.

The apparatus used to trap francium is based on the same principles as the one used to trap radioactive ^{87}Rb at Stony Brook [15, 16]. Beams of ^{18}O from the Stony Brook Superconducting LINAC are incident on the Au target mounted on a tungsten rod. The $^{197}\text{Au}(^{18}\text{O},xn)$ reaction at 100 MeV produces predominantly ^{210}Fr , which has a 3.2 min half-life. ^{210}Fr has an estimated α decay branching of $60 \pm 30\%$ with the remaining decays by β^+ or electron capture. The target is heated to $\approx 1200\text{K}$ by the beam power and by an auxiliary resistance heater. The elevated temperature is necessary for the alkali elements to rapidly diffuse to the surface and ionize. The francium surface-ionizes as it escapes from the gold because the work function of gold (4.8–5.1 eV) is larger than the ionization potential of francium (4.07 eV). A beam energy of 100 MeV is optimal for production of ^{210}Fr since this isotope is created very close to the surface facilitating its escape from the target. Changing the beam energy selects the production rate of the francium isotopes. Increasing the beam energy allows the francium nucleus to expel more neutrons during the cooling process following nuclear fusion. This produces francium isotopes with fewer neutrons closer to the gold surface. Heavy ion fusion reactions create $^{208-212}\text{Fr}$ isotopes with the reactions $^{16-18}\text{O}(^{197}\text{Au}, xn)^{208-211}\text{Fr}$, and $^{19}\text{F}(^{198}\text{Pt}, 5n)^{212}\text{Fr}$. We have captured $^{208,209,210,211,212}\text{Fr}$ in our MOT apparatus.

The francium ions enter the ion transport system (See Fig. 1). The target and electrodes are cylindrically symmetric to

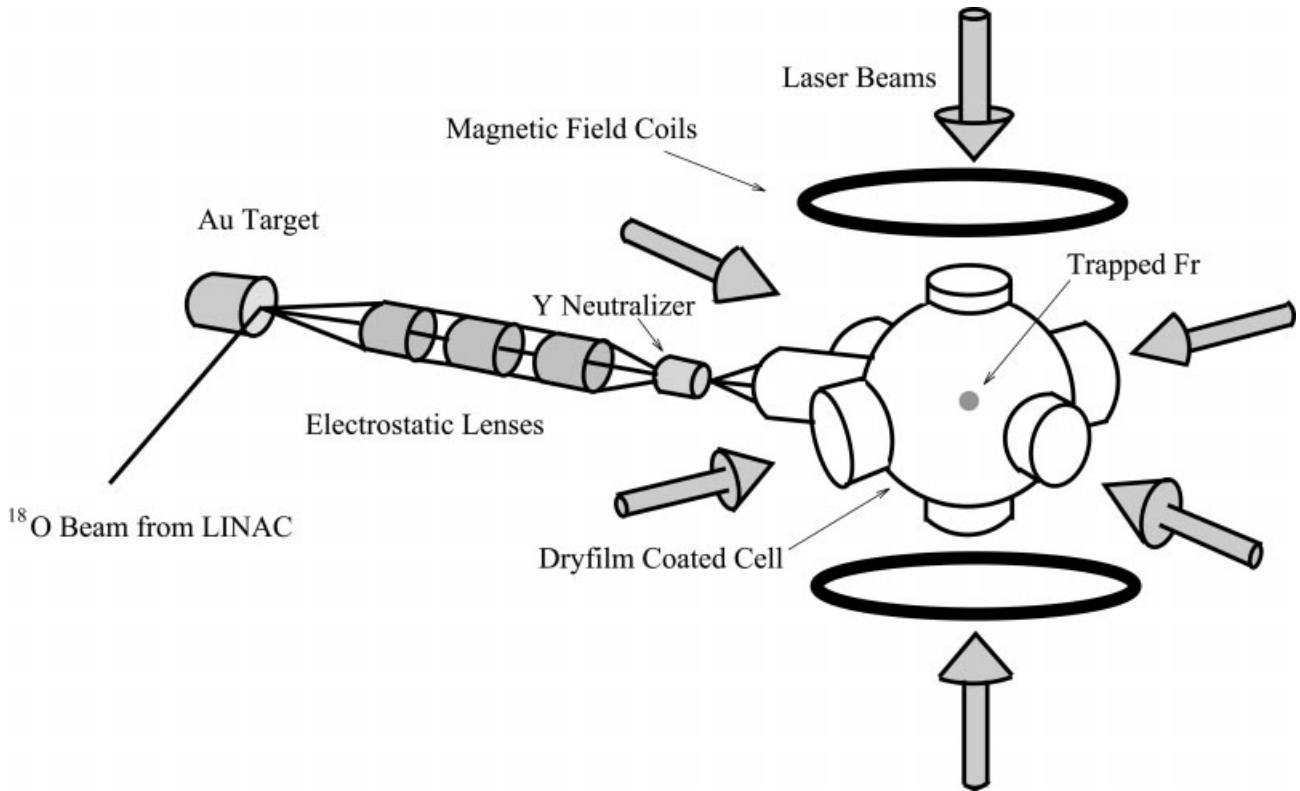


Fig. 1. Production, transport and capture apparatus for francium at Stony Brook.

reduce aberrations, and the ions are extracted at 135° from the ^{18}O beam direction. We measure the number of Fr ions in the beam by stopping them on a retractable plate (catcher) viewed by a silicon surface-barrier detector. We determine the number of francium atoms from the alpha-particle activity and the known solid angle of the detector. A beam from the Stony Brook Superconducting LINAC of 3×10^{12} ^{18}O ions/s on the Au produces $\approx 3 \times 10^6/\text{s}$ ^{210}Fr ions/s at the catcher.

At a temperature close to the melting point of gold (1336 K) the Fr diffuses rapidly to the surface, but the Au may melt. We have found a sensitive dependence of the number of francium ions on the target temperature. We have repeatedly observed a sharp increase in the number of francium ions that escape from a gold target when it is heated. Once the transition is reached a large increase in the francium escape rate occurs.

Separation of the production and the trapping regions is critical to operate the trap in a ultrahigh vacuum environment. Extracted at 800 V, the francium ions travel through three sets of electrostatic lenses that focus the ions and four sets of electrostatic plates that steer them. After about one meter, the ions pass through a differential-pumping aperture to the region of ultrahigh MOT vacuum. The ions land on the inner surface of a cylinder coated with yttrium that is heated to 970 K (melting point of Y = 1752 K). The low work function of Y (3.1 eV) results in the release of neutral Fr atoms from the Y surface that form an atomic beam directed towards the vapor cell MOT.

3. Fr atoms in a MOT

The francium trap consists of a 10 cm diameter Pyrex bulb with six 5 cm diameter windows and two viewing windows 3 cm in diameter. Six intersecting laser beams each with

$1/e^2$ (power) diameter of 4 cm and typical intensity of $7.8 \text{ mW}/\text{cm}^2$ form the MOT, together with a magnetic field gradient of $5.5 \times 10^{-2} \text{ T/m}$. The glass cell is coated with a non-stick Dry-film coating [17, 18] to allow the atoms multiple passes through the trapping region after thermalization with the walls [19]. The vapor-cell MOT captures the atoms from the low-velocity tail of the room-temperature Maxwell-Boltzmann distribution of atomic velocities.

The figure 2 shows the atomic energy levels of Fr relevant for trapping. A Coherent 899-21 titanium-sapphire laser excites the D_2 cycling transition $7S_{1/2}, F = 13/2 \rightarrow 7P_{3/2}, F = 15/2$ at 718 nm. The large ground-state hyperfine splitting (46.8 GHz in ^{210}Fr) requires an extra laser for repumping the atoms that fall into the $F = 11/2$ ground state. An EOSI

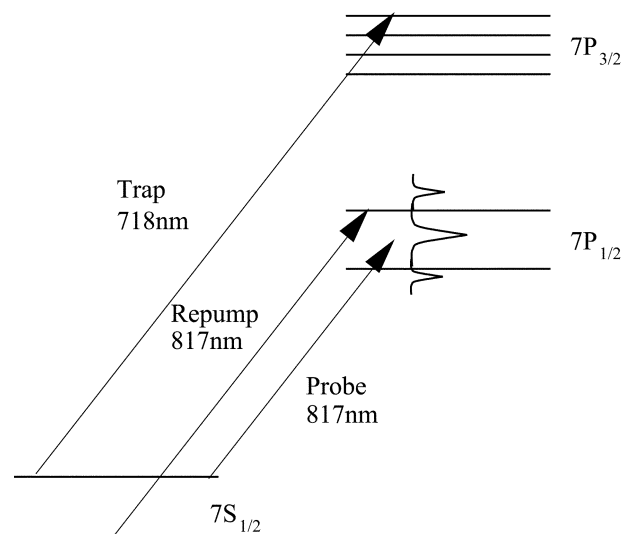


Fig. 2. Energy levels of Fr for trapping and spectroscopy. The sidebands on the probe laser used in the hyperfine splitting measurements of the $7P_{1/2}$ levels are indicated schematically.

2010 diode laser or a second Ti:Sapphire laser at 817 nm repump the atoms on the $7S_{1/2}$, $F = 11/2 \rightarrow 7P_{1/2}$, $F = 13/2$ transition.

4. Spectroscopy

The availability of a cold sample of Fr atoms has permitted us to study its spectroscopy with more detail than was possible in the past. We have located the first two excited states of the S manifold and measured the lifetime of the $7p$ levels. The following presents a very brief summary of those measurements with references to the complete work.

4.1 The $8S$ and $9S$ levels

We use a two photon processes to excite the atom from the $7S_{1/2} \rightarrow 7P_{3/2} \rightarrow 9S_{1/2}$ state [20] and the $7S_{1/2} \rightarrow 7P_{3/2} \rightarrow 8S_{1/2}$ state [21]. The trapping or repumping lasers provide the first photon and appropriate diode lasers provide the second. We photon count the decay with very good discrimination from any background.

The energy difference between the centers of gravity of the $9S_{1/2}$ level and the $7S_{1/2}$ ground state in ^{210}Fr is $25671.021 \pm 0.006 \text{ cm}^{-1}$. The center of gravity energy difference between the $7S_{1/2}$ ground level and the $8S_{1/2}$ level in ^{210}Fr is $19732.523 \pm 0.004 \text{ cm}^{-1}$. The hyperfine separation of the $8S_{1/2}$, $F = 11/2$ and $F = 13/2$ states is $10256 \pm 7 \text{ MHz}$ giving a magnetic dipole hyperfine constant A of $1577.8 \pm 1.1 \text{ MHz}$.

4.2 Lifetime of the $7p$ levels

We have performed lifetime measurements of the $7p^2P_{3/2}$ and $7p^2P_{1/2}$ levels of Fr [13, 22]. The time-correlated single-photon counting technique allows us to work with a small cold sample of ^{210}Fr atoms in a MOT. We excite the atoms with the trapping and repumping beams of the MOT and detect the decay of the atomic fluorescence. The results are a precision experimental test of the atomic many-body perturbation theory applied to the heaviest alkali. The lifetime results are 21.02(11) ns and 29.45(11) ns for the $7p^2P_{3/2}$ and $7p^2P_{1/2}$ levels respectively. This gives a line strength ratio, $S_{1/2}/S_{3/2}$, of 0.526(3) for these levels in Fr.

Ab initio calculations by the groups in New South Wales and Notre Dame [7, 9] agree with our measurements within the level of accuracy that they expect (1% for Ref. [7] and 2% for Ref. [9]). This comparison tests their ability to generate appropriate Fr wavefunctions. Other groups use semi-empirical methods and also obtain agreement with our measurements [10, 11, 12].

5. Hyperfine interval measurements

Our measurements of the hyperfine structure of the $7P_{1/2}$ level for $^{208-212}\text{Fr}$ have a precision of 300 ppm [24]. These measurements along with previous ground state hyperfine structure measurements reveal a hyperfine anomaly from the Bohr-Weisskopf effect [23]. We present in this section some of the experimental aspects that have made this precision possible, and refer the interested reader to the our recent paper [24] on the observation of a hyperfine anomaly and the strong sensitivity of the hyperfine anomaly to the radial distribution of the neutron magnetization.

5.1 Preliminaries

Precise measurements of hyperfine structure can probe the nuclear magnetization distribution. The Bohr-Weisskopf effect [23, 25] has been known for many years, but experimental and theoretical advances have now allowed more broadly based and detailed investigations [26, 27, 28, 29]. Comparison of adjacent isotopes allows extraction of the nuclear magnetization distribution of the last neutron, a quantity that is in general very difficult to study [30].

Bohr-Weisskopf effect measurements usually require detailed knowledge of both hyperfine structure constants and magnetic moments. Precision measurements of the hyperfine structure in atomic states with different radial distributions can give information on the hyperfine anomaly [31] and be sensitive to the nuclear magnetization distribution.

Coc *et al.* [32, 33] measured the $7S_{1/2}$ ground state hyperfine constants for 16 Fr isotopes, but only one magnetic moment has been measured [34]. We have focused on extracting hyperfine anomaly information using the available data in the literature and our new precision spectroscopy of the $7P_{1/2}$ hyperfine structure on five francium isotopes. Previous measurements of the hyperfine splitting of the $7P_{1/2}$ level [6, 33] were not of sufficient precision to observe the small hyperfine anomaly effects. The $7P_{1/2}$ electron probes the nucleus with a more uniform radial dependence of the interaction than does the $7S_{1/2}$ electron. The ratio of the hyperfine constants is sensitive to the nuclear magnetization distribution [31]. Since both states are spin- $\frac{1}{2}$, the measurements are independent of quadrupole effects that complicate the extraction of precise magnetic hyperfine structure constants.

The magnetic hyperfine interaction can be written as [25]

$$W_{\text{extended}}^l = W_{\text{point}}^l (1 + \varepsilon(A, l)) \quad (1)$$

where ε is a small quantity that depends on the particular isotope, A , and an atomic state, $l = S$ or P . The ratio, ρ , of hyperfine structure constants in the S and P states is given by

$$\begin{aligned} \rho_A &= \frac{W_{\text{extended}}^S}{W_{\text{extended}}^P} \\ &= \frac{W_{\text{point}}^S (1 + \varepsilon(A, S))}{W_{\text{point}}^P (1 + \varepsilon(A, P))}, \\ \rho_A &\approx \rho_0 (1 + \varepsilon(A, S) - \varepsilon(A, P)) \end{aligned} \quad (2)$$

where ρ_0 is the ratio of hyperfine structure constants for a point nucleus. Here, we have neglected the weak dependence of the hyperfine constants on the finite size of the charge distribution (Breit-Rosenthal effect). Equation (2) shows that the ratio ρ_A can have a different value for different isotopes because the S and P states have different sensitivity to the nuclear magnetization distribution. Since the error in the measurement comes from two hyperfine splittings, it is very important to have as accurate as possible numbers for especially the excited state splitting.

5.2 Experimental Method

Three Ti:Sapphire lasers excite different atomic transitions. Two lasers form the MOT: a trap laser on the D_2 cycling transition and a repump laser on the D_1 transition to

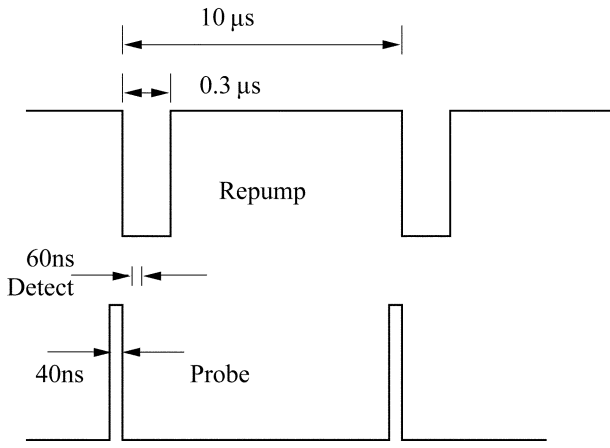


Fig. 3. Time sequence for excitation and detection of the $7P_{1/2}$ levels in Fr.

return atoms from the low F ground state to the trapping cycle [14]. We excite the hyperfine splitting of the $7P_{1/2}$ state with a 40 ns pulse from a third probe laser. We detect for 60 ns the fluorescence decay with an $f/1.5$ optical system and a Hamamatsu R636 photomultiplier. The repump laser is off for $0.3 \mu\text{s}$ during each cycle of $10 \mu\text{s}$.

This technique transfers the hyperfine splitting into a direct frequency measurement. We frequency modulate (FM) the probe laser with an electro-optic modulator. The resulting beam has FM sidebands at approximately $\pm 3 \text{ GHz}$ off the carrier. (See Figure 2).

The trapping laser, together with the repump laser keep a steady population on the higher hyperfine level of the ground state. Since we want to measure the hyperfine splitting of the excited state we turn off the repumper laser while we look for photons coming from the fluorescence of the $7P_{1/2}$ state on a time window that ensures minimal background contribution with maximal signal. (See Fig. 3 for the time sequence).

Figure 4 shows the schematic of the apparatus for the measurement. Fr does not have any stable isotope and the traditional techniques for locating and maintaining the lasers on the atomic transitions do not apply; however a computer controlled Fabry Perot cavity stabilizes and monitors the long term frequency of all of the lasers [35].

The sidebands on the probe laser excite the two hyperfine components of the $7P_{1/2}$ hyperfine splitting as we scan the carrier. The sidebands span most of the splitting and the carrier only has to scan a small frequency interval to reach

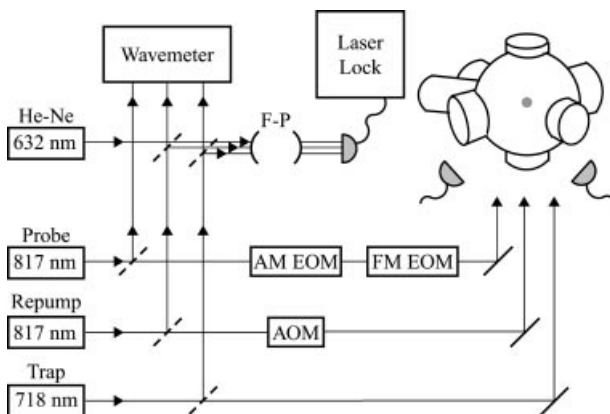


Fig. 4. Block diagram of the apparatus for the $7P_{1/2}$ hyperfine splitting measurement.

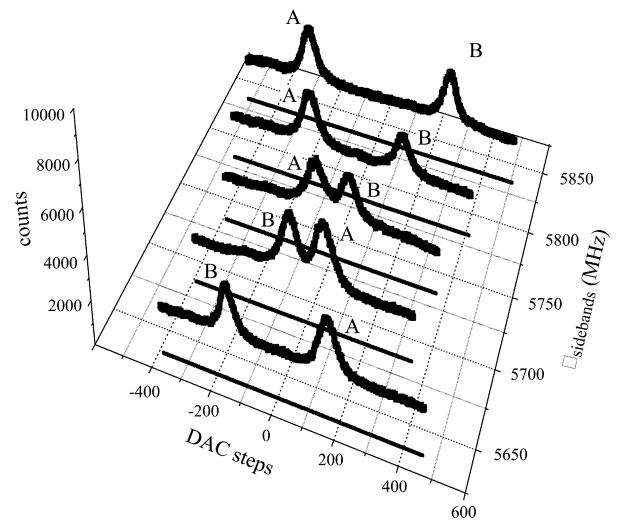


Fig. 5. Scans of the $7P_{1/2}$, $F=4$ and $F=5$ hyperfine states of ^{211}Fr . for five different RF frequencies. A and B identify the appropriate hyperfine states.

the two lines. We repeat the scans with different RF frequencies choosing values to have the sidebands larger or smaller than the hyperfine splitting. Figure 5 shows a series of five scans with changing RF frequency for ^{211}Fr . Each scan takes about 5 minutes to complete, with typical steps of 1 MHz/s .

The signal to noise ratio is larger than 50 in a single scan, so we can determine the peak of each scan with a precision of better than 0.5 MHz . We find the splitting by interpolating to zero on a least squares fit of the line positions versus the RF modulation frequency. The RF modulation frequency we obtain is directly the hyperfine splitting. Figure 6 shows an example of the data that we use in a fit as we follow the two hyperfine levels from Fig. 5. This figure is just the projection on the plane of the peaks from each scan.

The method does not rely on an absolute calibration of the scan rate of the laser and how it maps into the DAC steps. It relies on its stability from scan to scan, but the absolute calibration comes from the line intercept as a function of microwave frequency. This frequency is extremely stable and we measure it with a frequency counter.

Figure 7 shows our measurements of the hyperfine splitting of the $5P_{1/2}$ level of ^{87}Rb as a function of trap detuning.

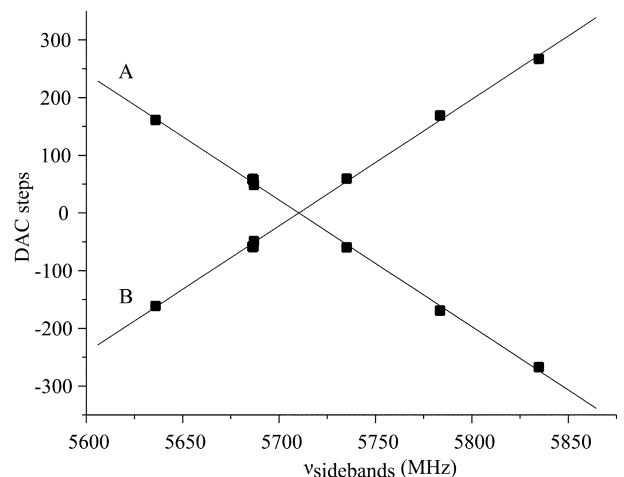


Fig. 6. Hyperfine resonant peak position as a function of RF modulation frequency for the $7P_{1/2}$, $F=4$ and $F=5$ hyperfine states of ^{211}Fr . A and B identify the appropriate hyperfine states.

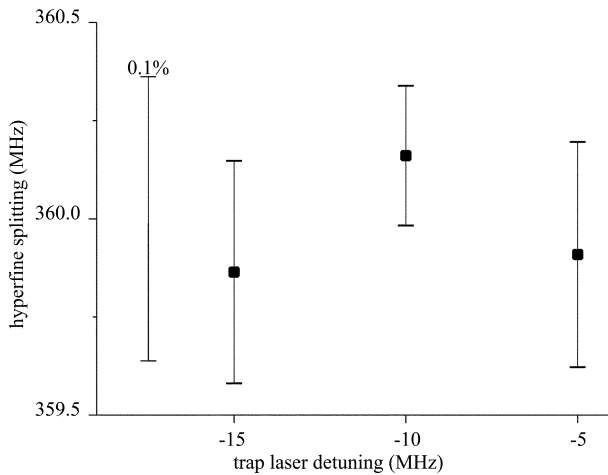


Fig. 7. Variation of the $5P_{1/2}$ hyperfine splitting in Rb as a function of trap detuning.

From tests like this one and others in francium we do not find any systematic dependence of the resonance positions with trap laser power, trap laser detuning, or probe laser power. Auxiliary experiments with Rb allow us to place an upper limit on a Zeeman shift of 0.8 MHz.

Figure 8 shows the ratios of the $7S_{1/2}$ to $7P_{1/2}$ hyperfine A constants for a series of isotopes of Fr. There is a distinctive even-odd alternation well beyond the size of our error bars. The qualitative explanation of this observation requires the use of radial distributions from recent theories, and we give more details in Ref. [24].

We have measured the hyperfine splitting of the $7P_{1/2}$ excited state in five Fr isotopes with a precision of 300 ppm. The results are sensitive to the radial distribution of the nuclear magnetization, and can be qualitatively understood within a simple picture where the effect is attributed to the unpaired nucleons, as identified by the shell model [24]. These measurements provide one of the few handles on the

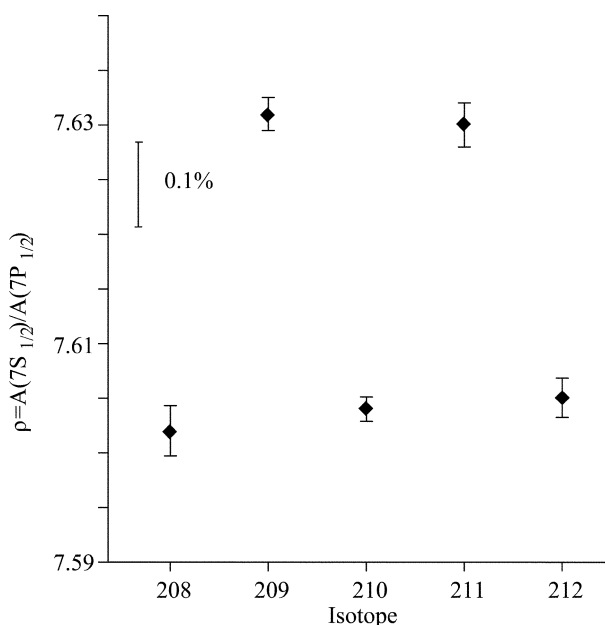


Fig. 8 Ratio of hyperfine A magnetic dipole constants of $7S_{1/2}$ and $7P_{1/2}$ states and differential changes observed for five different Fr isotopes. The S states come from the work of Coc *et al.* [32, 33] and the P states come from our work [24].

neutron radial distribution in nuclei, and will help to constrain nuclear structure calculations.

The light francium isotopes form a unique laboratory in which detailed calculations of both the nucleus and the atom are possible. More refined calculations in both systems should be able to eliminate many of the uncertainties which have clouded the understanding of the electron-nucleus interactions.

6. Future Work

Our francium work continues as an exploration of any other alkali. We are using a combination of tools from atomic, optical and nuclear physics to further understand this heavy element. The possibilities of precision spectroscopy to give information about particle physics, through a PNC measurement, are growing, and we expect to pursue the understanding of the heaviest alkali.

Acknowledgments

We would like to thank J. E. Simsarian and W. Z. Zhao for their contributions to this experiment. This work is supported by NSF.

References

1. Perey, M., C. R. Acad. Sci. **208**, 97 (1939).
2. Liberman, S. *et al.*, and the ISOLDE Collaboration, C. R. Acad. Sci. B **286**, 253 (1978).
3. For a sample and overview of the extensive work performed at ISOLDE see Arnold, E. *et al.* and the ISOLDE Collaboration, J. Phys. B **23**, 3511 (1990).
4. Andreev, S. V., Mishin, V. I. and Letokhov, V. S., J. Opt. Soc. Am. B **5**, 2190 (1988).
5. Simsarian, J. E. *et al.*, Phys. Rev. Lett. **76**, 3522 (1996).
6. Lu, Z.-T. *et al.*, Phys. Rev. Lett. **79**, 994 (1997).
7. Dzuba, V. A., Flambaum, V. V. and Sushkov, O. P., Phys. Rev. A **51**, 3454 (1995).
8. Dzuba, V. A., Flambaum, V. V. and Sushkov, O. P., J. Phys. B **17**, 1953 (1984).
9. Johnson, W. R., Liu, Z. W. and Sapirstein, J., At. Data Nucl. Data Tables **64**, 279 (1996).
10. Biémont, E., Quinet, P. and Van Renterghem, V., J. Phys. B **31**, 5301 (1998).
11. Marinescu, M., Vranceanu, D. and Sadeghpour, H. R., Phys. Rev. A **58**, 4259 (1998).
12. Van Wijngaarden, W. A. and Xia, J., J. Quant. Spectrosc. Radiat. Transfer **61**, 557 (1999).
13. See for example Simsarian, J. E., Orozco, L. A., Sprouse, G. D. and Zhao, W. Z., Phys. Rev. A **57**, 2448 (1998).
14. Sprouse G. D. and Orozco, L. A., Annu. Rev. Nucl. Part. Sci. **47**, 429 (1997).
15. Gwinner, G. *et al.*, Phys. Rev. Lett. **72**, 3795 (1994).
16. Behr, J. A. *et al.*, Nucl. Instr. and Meth. A **351**, 256 (1994).
17. Swenson D. R. and Anderson, L. W., Nucl. Instr. and Methods B **29**, 627 (1988).
18. Stephens, M., Rhodes, R. and Wieman, C., J. Appl. Phys. **76**, 3479 (1994).
19. Monroe, C., Swann, W., Robinson, H. and Wieman, C., Phys. Rev. Lett. **65**, 1571 (1990).
20. Simsarian, J. E., Shi, W., Orozco, L. A., Sprouse, G. D. and Zhao, W. Z., Opt. Lett. **21**, 1939 (1996).
21. Simsarian, J. E., Zhao, W. Z., Orozco, L. A. and Sprouse, G. D., Phys. Rev. A **59**, 195 (1999).
22. Zhao, W. Z., Simsarian, J. E., Orozco, L. A., Shi, W. and Sprouse, G. D., Phys. Rev. Lett. **78**, 4169 (1997).
23. Bohr, A. and Weisskopf, V. F., Phys. Rev. **77** 94 (1950).
24. Grossman, J. S. *et al.*, Phys. Rev. Lett. **83**, 935 (1999).
25. Stroke, H. H., Blin-Stoyle, R. J. and Jaccarino, V., Phys. Rev. **123**, 1326 (1961).

26. Mårtensson-Pendrill, A.-M., Phys. Rev. Lett. **74**, 2184 (1995).
27. Kühl, T. *et al.*, Nucl. Phys. A **626** 235 (1997).
28. Büttgenbach, S., Hyp. Int. **20**, 38 (1984).
29. Crespo Lopez-Urrutia, J. R. *et al.*, Phys. Rev. A **57** 879 (1998).
30. Duong, H. T. *et al.*, and the ISOLDE Collaboration, Nuc. Instr. and Meth. A **325**, 465 (1993).
31. Persson, J. R., Eur. Phys. J. A **2**, 4 (1998).
32. Coc, A. *et al.*, and the ISOLDE Collaboration, Phys. Lett. B **163**, 66 (1985).
33. Coc, A. *et al.*, and the ISOLDE Collaboration, Nucl. Phys A **468**, 1 (1987).
34. Ekström, C., Robertsson, L., Rosén, A. and the ISOLDE Collaboration, Physica Scripta **34**, 624 (1986).
35. Zhao, W. Z., Simsarian, J. E., Orozco, L. A. and Sprouse, G. D., Rev. Sci. Instr. **69**, 3737 (1998).